Counterflow and paired superfluidity in one-dimensional Bose mixtures in optical lattices

Anzi Hu,[1] L. Mathey,[1] Ippei Danshita,[2,3] Eite Tiesinga,[1] Carl J. Williams,[1] and Charles W. Clark[1]

[1]*Joint Quantum Institute, University of Maryland and National Institute of Standards and Technology, Gaithersburg, Maryland 20899, USA*

[2]*Department of Physics, Faculty of Science, Tokyo University of Science, Shinjuku-ku, Tokyo 162-8601, Japan*

[3]*Department of Physics, Boston University, Boston, Massachusetts 02215, USA*

We study the quantum phases of mixtures of ultracold bosonic atoms held in an optical lattice that confines motion or hopping to one spatial dimension. The phases are found by using the Tomonaga-Luttinger liquid theory as well as the numerical method of time-evolving block decimation (TEBD). We consider a binary mixture of equal density with repulsive intraspecies interactions and either repulsive or attractive interspecies interaction. For a homogeneous system, we find paired and counterflow superfluid phases at different filling and hopping energies. We also predict parameter regions in which these types of superfluid order coexist with charge-density wave order. We show that the Tomonaga-Luttinger liquid theory and the TEBD qualitatively agree on the location of the phase boundary to superfluidity. We then describe how these phases are modified and can be detected when an additional harmonic trap is present. In particular, we show how experimentally measurable quantities, such as time-of-flight images and the structure factor, can be used to distinguish the quantum phases. Finally, we suggest applying a Feshbach ramp to detect the paired superfluid state and a $\pi/2$ pulse followed by Bragg spectroscopy to detect the counterflow superfluid phase.

I. INTRODUCTION

Bose-Einstein condensation (BEC) [1] is a fascinating many-body phenomenon. It demonstrates the significance of quantum statistics at low temperature. Identical bosons can occupy the same single-particle state and are in fact more likely to do so than classical particles. At a critical temperature, a gas of bosons undergoes a phase transition toward a state in which a macroscopic fraction of the particles occupy the lowest-energy state, creating a condensate. Such a state was realized in ultracold atom systems in [2], demonstrating that the technology of cooling and manipulating atoms had reached a level of control with which novel states of matter could be generated and studied.

In the case of a Fermi gas, the Pauli exclusion principle prevents such a phenomenon from occurring, because no single-particle state can be more than singly occupied. However, the phenomenon of condensation can still occur in Fermi systems via a different mechanism: fermions can form pairs to create composite bosons. The bosonic particles can then form a condensate of pairs. Conventional superconductors, for example, were understood as a condensate of electron pairs [3]. In ultracold atoms, fermionic condensates of this type were created in [4].

Interestingly, this mechanism of condensation of pairs is not limited to fermionic systems but can occur in bosonic systems as well. In fermionic systems, formation of bosonic pairs necessarily occurs before condensation. In bosonic systems this mechanism can be favored energetically and will typically be in competition with single-particle condensation.

In Refs. [5,6], two types of composite bosons were predicted for a binary Bose mixture in an optical lattice: pairs and antipairs. For attractive mutual interactions, a bosonic mixture can form pairs of atoms which then form a paired superfluid (PSF) state, as is visualized in Fig. 1. For repulsive interactions, at special fillings, the atoms can form antipairs, which can be interpreted as pairs of one atom of one species and one hole of the other species. These antipairs can then generate a counterflow superfluid (CFSF) state visualized in Fig. 2. Most of their simulations were performed for two-dimensional (2D) systems.

Quantum phases of atoms in optical lattices have been experimentally studied. Following the prediction by Jaksch *et al.* in [7], the Mott insulator (MI)-to-superfluid (SF) transition was realized in Ref. [8] in a three-dimensional lattice. In [9] this transition was achieved in one dimension. More recently, Ref. [10] observed the 2D transition.

In one-dimensional (1D) gases quantum phases have quasi-long-range order, rather than true long-range order. A quasi-long-range order of an order parameter operator $O(x)$ is defined as follows: the correlation function $R(x) = \langle O^\dagger(x)O(0) \rangle$ falls off algebraically as $R(x) \sim |x|^{\alpha-2}$ as $|x| \to \infty$ with $0 < \alpha < 2$. A positive α implies a diverging susceptibility of the operator $O(x)$ (see, e.g., [11]). Various order parameters $O(x)$ will be defined in the text. In contrast in
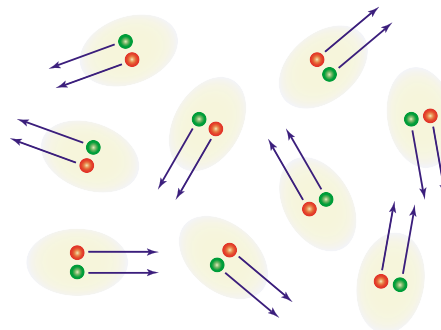
FIG. 1. (Color online) Sketch of a condensate of pairs. Atoms of each species (red and green bullets) pair together and form a PSF state.
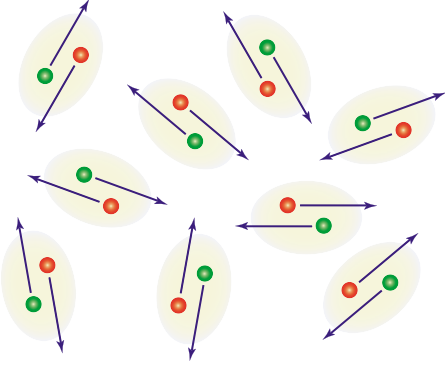
FIG. 2. (Color online) Sketch of a condensate of antipairs. Here, atoms of one species are strongly anticorrelated with atoms of the other species, creating a CFSF state. These composite bosons can also be thought of as a pair of one atom of one species and one hole of the other species.

higher-dimensional bosonic systems correlation functions can have true long-range order, where correlation functions approach a finite value. Power-law scaling in a 1D optical lattice has been observed in Ref. [12]. They observed the Tonks-Girardeau regime of strongly interacting bosons.

In this paper we consider a two-component Bose mixture held in an optical lattice that only allows atoms to hop in one spatial dimension. We ask the question of how the superfluid as well as other phases or orders can be realized. We assume that the two species of the mixture have the same filling ν, restricted to the range $0 < \nu \leq 1$. The phase diagram of these mixtures is determined using the Tomonaga-Luttinger liquid theory [11,13], which gives the universal phase diagram in terms of a few effective parameters. Based on the universal phase diagram, we generate the numerical phase diagram using the time-evolving block decimation (TEBD) method [14–17]. With these two approaches, we find that CFSF can exist for $\nu = 1/2$ (half-filling) and repulsive interaction, whereas PSF can exist for $\nu < 1$ and attractive interaction (see also [18]). As CFSF can be interpreted as a superfluid of pairs of one particle of one species and a hole of the other, it naturally occurs at half-filling where the numbers of particles and holes are the same. This theory can be generalized to unequal filling fractions. In this case, PSF does not occur. However, when the filling fractions add up to 1, CFSF can occur [19].

We also find that charge-density wave (CDW) quasiorder can coexist with both PSF and CFSF, as well as single-particle superfluidity (SF). The regimes in which CDW and SF quasiorder coexist constitute a quasisupersolid phase [20,21]. Similarly, the regimes where CDW and PSF quasiorder coexist are a quasisupersolid of pairs and, in the case of CFSF, a quasisupersolid of antipairs. Previous work has predicted coexistence of CDW and PSF for 1D Bose mixtures [19,20] and bilayer 2D lattice bosons with long-range interactions [22], and that of CDW and CFSF for 1D Bose-Fermi mixtures [21,23].

We then address the question whether PSF and CFSF can be realized and detected in experiment. To simulate the effect of a global trap, we numerically study a mixture confined by a harmonic trap and find that PSF and CFSF can indeed exist

in such trapped systems. Their existence can be detected through various measurements. The PSF phase can be detected by using a Feshbach ramp, similar to what has been used in BEC-BCS experiments [4], which generates a quasi-condensate signal in the resulting molecules. The CFSF phase can be detected by applying a $\pi/2$ pulse followed by Bragg spectroscopy. This generates a quasicondensate signal in the structure factor. Time-of-flight (TOF) expansion can also be used to show the absence of single-particle superfluidity in PSF and CFSF. Measuring the structure factor via Bragg spectroscopy can be one way of detecting CDW order.

This paper is organized as follows: in Sec. II, we introduce the model that is used to describe the system; in Sec. III, we use the Tomonaga-Luttinger liquid theory to derive the phase diagram. The numerical approach and results are discussed in Sec. IV. Specifically, phase diagrams of the homogeneous system are presented in Sec. IV A, and the realization and the detection of PSF and CFSF are discussed in Sec. IV B. We conclude in Sec. V.

II. HAMILTONIAN

Ultracold bosonic atoms in optical lattices can be well described by Bose-Hubbard models [7]. Here, we consider a mixture of two types of atoms confined to a one-dimensional lattice system. The Hamiltonian of such a system is given by

$$H = -t \sum_{a=1,2} \sum_{j=1}^{N-1} (b_{a,j}^\dagger b_{a,j+1} + \text{H.c.}) + U_{12} \sum_{j=1}^{N} n_{1,i} n_{2,i}$$
$$+ \frac{U}{2} \sum_{a=1,2} \sum_{i=1}^{N} n_{a,i}(n_{a,i} - 1). \tag{1}$$

We denote the different types of atoms with index $a = 1, 2$ and the lattice site with index i. We assume that the two species have equal particle density $\nu \leq 1$, the same intraspecies interaction $U > 0$ and hopping parameter $t > 0$. The interspecies interaction is given by U_{12}. The operators $b_{a,i}^\dagger$ and $b_{a,i}$ are the creation and the annihilation operators for atoms of type a and site i and $n_{a,i} = b_{a,i}^\dagger b_{a,i}$ are the number operators.

III. TOMONAGA-LUTTINGER LIQUID APPROACH

The universal behavior of this system can be found within a Tomonaga-Luttinger liquid description [11]. In this paper, we are interested in the phase diagram of the system at various densities and interactions. First, we switch to a continuum description, $b_{a,i} \rightarrow b_a(x)$, and express the operators $b_a(x)$ through a bosonization identity, according to Haldane [24,25],

$$b_a(x) = [n + \Pi_a(x)]^{1/2} \sum_m e^{2mi\Theta_a(x)} e^{i\phi_a(x)}, \tag{2}$$

where the real-space density of each species is $n = \nu/a_L$ and a_L is the lattice constant. The lattice sites are at positions $x = ia_L$. This expression is a phase-density representation of the Bose operators, in which the square root of the density operator has been written in an intricate way. The fields $\Pi_{1,2}(x)$ describe the small amplitude and the long-

wavelength density fluctuations. The fields $\Theta_{1,2}(x)$ are given by $\Theta_{1,2}(x) = \pi n x + \theta_{1,2}(x)$, where $\theta_{1,2}(x) = \pi \int^x dy \, \Pi_{1,2}(y)$. The fields $\phi_{1,2}(x)$ describe the phase and are conjugate to the density fluctuations $\Pi_{1,2}(x)$.

The contact interactions between the densities in (1) written in Haldane's representation generate an infinite series of terms that contain $\exp[2m_1 i(\pi n x + \theta_1) + 2m_2 i(\pi n x + \theta_2)]$, where m_1 and m_2 are some integers. A term of this form can only drive a phase transition if the oscillatory part $2\pi m_1 n x + 2\pi m_2 n x$ vanishes for all lattice sites. This leads to the requirement $m_1 \nu + m_2 \nu = m_3$, with m_3 as another integer [19]. As a further requirement, small integers m_1 and m_2 are necessary, because the scaling dimension of the term scales quadratically in m_1 and m_2.

For the range $0 < \nu \leq 1$, we find that there are three different cases: unit filling ($\nu = 1$), half-filling ($\nu = 1/2$), and noncommensurate filling ($\nu \neq 1$ and $\nu \neq 1/2$). It can be checked, using renormalization-group (RG) arguments as below that higher forms of commensurability do not generate new phases, but that either phase separation (PS) or collapse (CL) is reached first. Our numerical findings are consistent with this.

A. Noncommensurate filling

The action of the system, assuming a short-range spatial cutoff r_0, at noncommensurate filling is given by [11,20,25]

$$S = \int d^2r \left[\sum_{j=1,2} \frac{1}{2\pi K} [(\partial_{v\tau}\theta_j)^2 + (\partial_x \theta_j)^2] + \frac{U_{12}a_L}{\pi^2 v \hbar} \partial_x \theta_1 \partial_x \theta_2 \right.$$
$$\left. + \frac{2g_\sigma}{(2\pi r_0)^2} \cos(2\theta_1 - 2\theta_2) \right] \quad (3)$$

The first line of the action is characterized by a Luttinger parameter K and a velocity v, contained in $\mathbf{r} = (v\tau, x)$. This part of the action, without the coupling between the two fields $\theta_a(x)$, generates a linear dispersion $\omega = v|k|$, where v should therefore be interpreted as the phonon velocity. The Luttinger parameter K is a measure of the intraspecies interaction U. We will be interested in the regime $U \gtrsim t$, in which we have approximately [26]

$$K \approx 1 + \frac{8t}{U} \frac{\sin \pi \nu}{\pi}. \quad (4)$$

The velocity v can also be related to the parameters of the underlying Hubbard model by

$$v \approx v_F(1 - 8t\nu \cos \pi\nu/U), \quad (5)$$

where v_F is the "Fermi velocity" of an identical system of fermions, $v_F = 2(a_L t/\hbar)\sin \pi\nu$, and k_F is the "Fermi wave vector" $k_F = \pi n$. Here, $\hbar$ is the Planck constant.

The two fields $\theta_a(x)$ are coupled by the interspecies interaction. The interaction term $U_{12}n_1 n_2$ in the underlying Hubbard model generates both the term containing $\partial_x \theta_1 \partial_x \theta_2$, as well as the backscattering term [11,19] containing $\cos(2\theta_1 - 2\theta_2)$. The action S is only well defined with a short-range cutoff r_0. It is proportional to $1/n$. At this scale, g_σ is approximately given by

$$g_\sigma = U_{12}a_L/(v\hbar). \quad (6)$$

We diagonalize the quadratic part of the action by switching to the symmetric and the antisymmetric combinations $\theta_{S/A} = \frac{1}{\sqrt{2}}(\theta_1 \pm \theta_2)$. For the two sectors we find

$$K_{S/A} = [1/K^2 \pm U_{12}a_L/(v\hbar\pi K)]^{-1/2} \quad (7)$$

as effective Luttinger parameters. To lowest order in U_{12}, this gives $K_{S/A} \approx K \mp U_{12}a_L K^2/(2\pi v\hbar)$. The effective velocities are $v_{S/A} = v\sqrt{1 \pm U_{12}a_L K/(\pi v\hbar)}$. The collapse (phase separation) of the superfluid phase is when $v_{S/A}$ is imaginary. We note that K_S diverges when CL is approached, and that K_A diverges as the system approaches PS.

After the diagonalization, the action is quadratic in θ_S and does not couple θ_S and θ_A. We therefore focus on the antisymmetric sector which contains the nonlinear backscattering term $\cos(2\sqrt{2}\theta_A)$. To study its effect, we use an RG approach. We renormalize the short-range cutoff r_0 to a slightly larger value and correct for it at one-loop order. The resulting flow equations are given by [11]

$$\frac{dg_\sigma}{dl} = (2 - 2K_A)g_\sigma, \quad (8)$$

$$\frac{dK_A}{dl} = -\frac{g_\sigma^2}{2\pi^2}K_A^3. \quad (9)$$

The flow parameter l is given by

$$l = \log_e\left(\frac{r_0'}{r_0}\right), \quad (10)$$

where r_0' is the cutoff that has been created in the RG process.

The flow equations (8) and (9) have two qualitatively different fixed points: either g_σ diverges, which in turn renormalizes K_A to zero, or g_σ is renormalized to zero for finite $K_A = K_A^*$. In the latter case, the action S is quadratic in θ_S and θ_A. For the parameter K_S, we use the bare value given in Eq. (7).

As mentioned in the Introduction, we can determine the phase diagram by studying the long-range scaling behavior of correlation functions, $\langle O^\dagger(x)O(y)\rangle$, of various order parameters $O(x)$. In particular, the single-particle superfluid order parameter is $O_{SF} = b_a(x)$ with $a = 1, 2$. The CDW order is related to the $2k_F$ wave-vector component of the density operator, $O_{CDW} = n_a$. PSF is described by $O_{PSF} = b_1(x)b_2(x)$ and CFSF is described by $O_{CFSF} = b_1^\dagger(x)b_2(x)$. In the homogeneous system, it suffices to study

$$G(x) = \langle b_a^\dagger(x)b_a(0)\rangle, \quad a = 1,2, \quad (11)$$

$$R_{n,a}(x) = \langle n_a(x)n_a(0)\rangle, \quad a = 1,2, \quad (12)$$

$$R_S(x) = \langle b_1^\dagger(x)b_2^\dagger(x)b_1(0)b_2(0)\rangle, \quad (13)$$

$$R_A(x) = \langle b_1^\dagger(x)b_2(x)b_1(0)b_2^\dagger(0)\rangle. \quad (14)$$

We find that, away from CL and PS, the correlation functions scale either algebraically or exponentially. For algebraic scaling, we have

TABLE I. Definitions of Mott insulator (MI), superfluid (SF), counterflow superfluid (CFSF), and paired superfluid (PSF) orders in terms of the long-range behavior of the correlation functions $R_S(x)$, $R_A(x)$, and $G(x)$. Each of these can either show algebraic (alg.) decay with scaling exponents between zero and two or exponential (exp.) decay with scaling exponents approaching $-\infty$. When K_S or K_A diverges, the system is either collapsed (CL) or phase separated (PS). CDW quasi-long-range order, which is determined by the long-range behavior of $R_{n,a}$, only exists for $0 < \alpha_{CDW} < 2$. It can coexist with each of the superfluid orders.

	$R_S(x)$	$R_A(x)$	$G(x)$
MI	Exp.	Exp.	Exp.
SF	Alg.	Alg.	Alg.
CFSF	Exp.	Alg.	Exp.
PSF	Alg.	Exp.	Exp.
CL or PS	$R_S(x)$, $R_A(x)$ undefined		

$$G(x) \sim |x|^{\alpha_{SF}-2}, \quad \alpha_{SF} = 2 - 1/(4K_S^*) - 1/(4K_A^*), \quad (15)$$

$$R_{n,a}(x) \sim \cos(2k_Fx)|x|^{\alpha_{CDW}-2}, \quad \alpha_{CDW} = 2 - K_S^* - K_A^*, \quad (16)$$

$$R_S(x) \sim |x|^{\alpha_{PSF}-2}, \quad \alpha_{PSF} = 2 - 1/K_S^*, \quad (17)$$

$$R_A(x) \sim |x|^{\alpha_{CFSF}-2}, \quad \alpha_{CFSF} = 2 - 1/K_A^*, \quad (18)$$

where the scaling exponents α are determined by K_S^* and K_A^*, which are the values of K_S and K_A after the RG flow. For the case that g_σ diverges in Eqs. (8) and (9) and K_A is undefined, these expressions can still be used. We set K_A to zero and find that α_{CDW} and α_{PSF} are well defined. Hence, $R_{n,a}$ and R_S still show algebraic scaling. On the other hand, α_{CFSF} and α_{SF} become $-\infty$ and G and R_A scale exponentially.

We can identify regimes where different scaling exponents are positive based on the relationship between the scaling exponents and $K_{S/A}$ after the flow. This determines the different quasi-long-range orders that are present. The relationships are summarized in Table I. The resulting phase diagram is shown in Fig. 3, as a function K and $U_{12}a_L/(v\hbar)$, as appearing in the action in Eq. (3). These two parameters determine the initial values of the flow equations through Eqs. (7) and (6).

We can estimate the phase boundary between PSF and SF. This phase boundary is where the single-particle phases lose their quasi-long-range order. Because the single-particle phases have exponential scaling if either ϕ_A or ϕ_S has exponential scaling (note that, e.g., $e^{i\phi_1(x)}e^{-i\phi_1(y)} = e^{i[\phi_A(x)-\phi_A(y)]/\sqrt{2}}e^{i[\phi_S(x)-\phi_S(y)]/\sqrt{2}}$), this phase boundary is where R_A shows exponentially decay. This transition is a Berezinskii-Kosterlitz-Thouless transition [27]. For small $U_{12}a_L/(v\hbar)$, this boundary is near the point $K_A = 1$ and $g_\sigma = 0$. For that limit, Eq. (9) can be linearized to
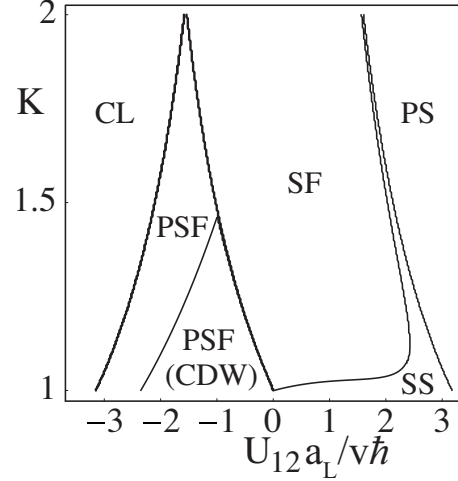
FIG. 3. Phase diagram of a bosonic mixture at nonunit and non-half-filling as a function of the bare parameters K and U_{12}. For attractive interactions U_{12} and $K < 2$, the system can form a paired superfluid state, in the regime labeled PSF and PSF (CDW). This phase can coexist with CDW order for weaker interactions. For large repulsive (attractive) interactions U_{12}, the system phase separates (PS) [collapses (CL)]. For the remaining regime, the system shows single-particle superfluidity (SF). This can coexist with CDW order, resulting in a quasisupersolid (SS) regime. Note that the filling only enters through the value of K and is not specified independently.

$$\frac{dK_A}{dl} = -\frac{g_\sigma^2}{2\pi^2} \quad (19)$$

and the expression $A = \pi^2(1-K_A)^2 - g_\sigma^2/4$ becomes an invariant of the flow. From the properties of the RG flow of a Berezinskii-Kosterlitz-Thouless transition (see, e.g., [11,27]), the phase boundary is given by $A = 0$ and $g_\sigma < 0$. Using the expressions of K_A and v in terms of the Hubbard parameters, we estimate the critical interaction U_{12} for PSF to occur at

$$\left.\frac{U_{12}}{U}\right|_c = -32\frac{t^2}{U^2}\sin^2(\pi v). \quad (20)$$

We also find that CDW can coexist with the PSF order for attractive interaction U_{12} and with SF order for repulsive U_{12}. These regimes are determined based on the condition $\alpha_{CDW} > 0$. In PSF regime, because K_A is formally set to zero, the value of α_{CDW} only depends on the value of K_S and is positive when $K_S < 2$. However, because of the jump of K_A from 0 to 1 at the PSF-SF boundary, the value of α_{CDW} is suddenly decreased by 1. This leads to the absence of CDW order in the SF regime for attractive U_{12}. On the repulsive side we find coexistence of SF and CDW order, which constitutes a quasisupersolid phase. The phase boundary between supersolid and SF has been estimated in Ref. [20]. In general, CDW order is more likely to occur for smaller values of K, because the system is "less superfluid" in this regime and has a stronger tendency to form periodic order, as can be seen in Fig. 3.
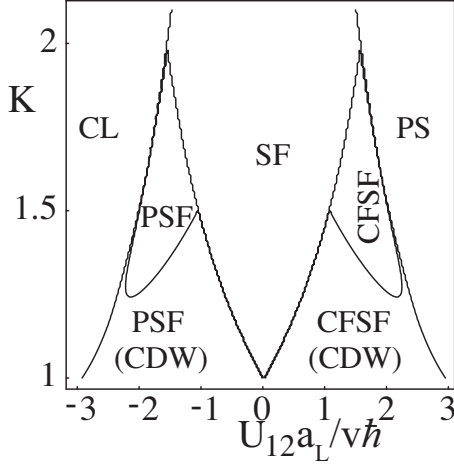
FIG. 4. Phase diagram of a bosonic mixture at half-filling as a function of the bare parameters K and U_{12}. In addition to the phases that appear in Fig. 3, the system now develops a CFSF phase, which can coexist with CDW order. Note that the filling only enters through the value of K and is not specified independently.

B. Half-filling

In the case where both species have a filling fraction of $1/2$ per site, another nonlinear term has to be introduced in the action

$$S_{uk} = \frac{2g_{uk}}{(2\pi r_0)^2}\int d^2r\, \cos(2\theta_1 + 2\theta_2). \qquad (21)$$

This term describes umklapp scattering. At the initial cutoff $r_0 \sim 1/n$, g_{uk} is approximately given by $U_{12}a_L/v$. In addition to the RG flow in the antisymmetric sector, we now also have

$$\frac{dg_{uk}}{dl} = (2 - 2K_S)g_{uk}, \qquad (22)$$

$$\frac{dK_S}{dl} = -\frac{g_{uk}^2}{2\pi^2}K_S^3 \qquad (23)$$

in the symmetric sector. Proceeding along the same lines as for the noncommensurate case, we find the phase diagram shown in Fig. 4. We note that terms such as $\int \cos(4\theta_{1,2})$ can also appear in the action at half-filling. However, we find that their scaling dimensions are too large to be relevant for a Hubbard model. Our numerical findings are consistent with this.

We estimate the SF-CFSF phase boundary in the same way as the PSF-SF boundary. We find

$$\left.\frac{U_{12}}{U}\right|_c = 32\frac{t^2}{U^2}\sin^2(\pi\nu). \qquad (24)$$

We note that the compressibility of the total density is given by

$$\kappa = \frac{2K_S}{\pi v_S} \qquad (25)$$

(see, e.g., [11]). From this expression, we can see that the compressibility vanishes in the CFSF regime, because K_S is renormalized to zero. This can also be related to the opening of a charge gap in the CFSF regime

C. Unit filling

In the case where both species have a filling fraction of one atom per site, we have to introduce a term of the form

$$S_1 = \frac{2g_1}{(2\pi r_0)^2}\int d^2r[\cos(2\theta_1) + \cos(2\theta_2)]. \qquad (26)$$

The resulting RG flow for this system is given by

$$\frac{dg_{uk}}{dl} = (2 - 2K_S)g_{uk} + \alpha_3 \frac{g_1^2(K_A - K_S)}{2\pi}, \qquad (27)$$

$$\frac{dg_\sigma}{dl} = (2 - 2K_A)g_\sigma + \alpha_3 \frac{g_1^2(K_S - K_A)}{2\pi}, \qquad (28)$$

$$\frac{dg_1}{dl} = \left(2 - \frac{K_S + K_A}{2} + \alpha_3 \frac{g_{uk}K_S + g_\sigma K_A}{\pi}\right)g_1, \qquad (29)$$

$$\frac{dK_A}{dl} = -\frac{g_\sigma^2}{2\pi^2}K_A^3 - \frac{g_1^2}{16\pi^2}(K_S + K_A)K_A^2, \qquad (30)$$

$$\frac{dK_S}{dl} = -\frac{g_{uk}^2}{2\pi^2}K_S^3 - \frac{g_1^2}{16\pi^2}(K_S + K_A)K_S^2, \qquad (31)$$

where α_3 is some nonuniversal parameter [28]. The behavior of this set of equations depends strongly on the initial value of g_1. For small values of g_1, four phases can be stable: single-particle superfluidity, CFSF, PSF, and a Mott phase. For large values only single-particle SF and MI are stable. We determine with our numerical approach that the Hubbard model falls into the second category, i.e., there is only a single-particle SF and a Mott state at unit filling.

Having established the universal behavior of the system from the Tomonaga-Luttinger liquid theory, we now want to connect the phase diagram with the parameters in the Hubbard model. The expressions (4) and (5), which relate the Luttinger parameter K and the velocity v to microscopic parameters of the Hubbard model, are only approximate and no full analytical expression is known. In addition, only some phase boundaries are predicted reliably, because we use perturbative RG in the g_σ. We expect that the analytical calculation only predicts the general structure of the phase diagram, as well as the decay behavior of the correlation functions. To obtain the phase diagram in terms of the parameters in the Hubbard model, we need to use numerical methods. The next section describes the numerical determination of the phase diagram.

IV. NUMERICAL APPROACH

We use the TEBD method [14] to study our discrete one-dimensional two-species Hubbard Hamiltonian. With this
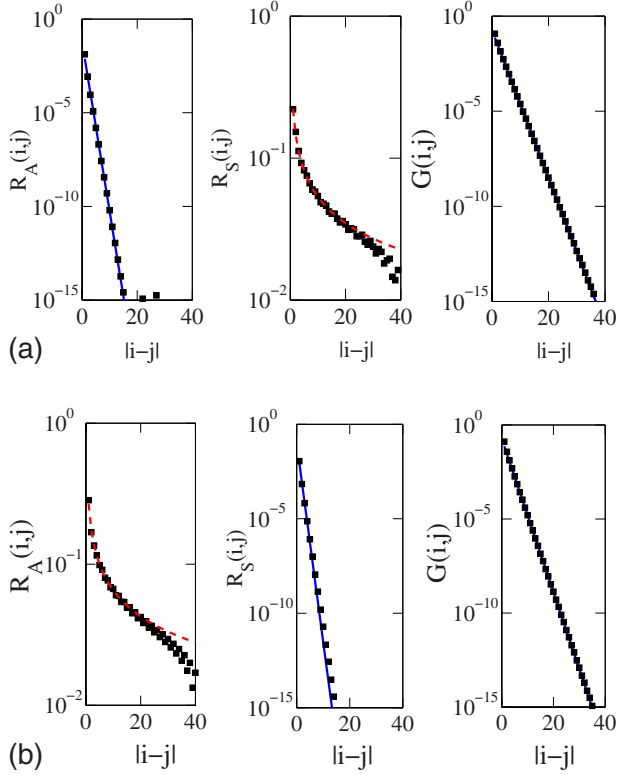
FIG. 5. (Color online) The correlation functions R_A, R_S, and G on a logarithmic scale as a function of distance $|i-j|$. The index i is 40, the center of the 80 lattice sites. The squares are the numerical data. The blue lines are exponential fits to the data and red dotted lines are algebraic fits. Note that the scale of the vertical axis of the graphs differs by orders of magnitude. In (a), we show an example for the paired superfluid phase at $\nu=0.3$, $t=0.02U$, and $U_{12}=-0.16U$. R_A decays exponentially and R_S decays algebraically. The single-particle correlation function decays exponentially, implying the absence of single-particle superfluidity. In (b), we show an example for the counterflow superfluid phase at $\nu=0.5$, $t=0.02U$, and $U_{12}=0.2U$. The antipair correlation function R_A decays algebraically, while the pair correlation function decays exponentially. Single-particle superfluidity is again absent. The algebraic fits deviate from the data around $|i-j|\approx 40$ due to the boundary conditions of our numerical calculations.

method, explained in the Appendix, we obtain an approximate ground-state solution. We consider N lattice sites with hard-wall boundary conditions and express the Hubbard parameters in units of the intraspecies interaction U. The number of sites N is equal to 80, unless otherwise noted. In our numerical analysis, we limit the particle number on each site and each species to two for filling $\nu \leq 0.8$ and hopping energy $t \leq 0.1U$ and four otherwise. Once we obtain the ground state, we calculate the energy, the density distributions, the correlation functions, and the structure factor to identify the quasi-long-range order and other properties of the ground state.

In Figs. 5(a) and 5(b), we show the decay behavior of the correlation functions in the PSF and the CFSF phases, respectively. As the Hamiltonian is discrete, the correlation functions are calculated as discrete functions: $G(i,j)=\langle b_{a,i}^{\dagger} b_{a,j} \rangle$, $R_S(i,j)=\langle b_{1,i}^{\dagger} b_{2,i}^{\dagger} b_{1,j} b_{2,j} \rangle$, and $R_A(i,j)$

$=\langle b_{1,i}^{\dagger} b_{2,i} b_{1,j} b_{2,j}^{\dagger} \rangle$. For the PSF phase, $R_A(i,j)$ decays exponentially, while R_S decays algebraically. It is also worthwhile to notice that the single-particle Green's function decays *exponentially*, implying the absence of single-particle superfluidity. For the CFSF phase, R_A decays algebraically while R_S decays exponentially. Single-particle superfluidity is again absent.

Behavior of K_S and K_A. We now study the decay behavior of R_S and R_A in more detail. Using the fit function, $c|i-j|^{\alpha-2}$, where c and α are the fitting parameters, we obtain the power-law exponent α and, hence, the Luttinger parameters K_S and K_A based on Eqs. (17) and (18). In Fig. 6(a), we show these K_S and K_A as functions of U_{12} for filling at 0.7 and t at $0.02U$. A Luttinger parameter is formally set to zero when its correlation function decays exponentially.

For $U_{12}<-0.06U$, R_A decays exponentially, while for $U_{12}>-0.06U$, R_A decays algebraically and K_A increases as U_{12} increases. The system undergoes a PSF-to-SF transition at $U_{12}=-0.06U$. On the other hand, K_S decreases monotonically for $U_{12}>-0.6U$. For $U_{12}<-0.6U$ the numerics failed to converge to a homogeneous state. This indicates that the system collapses, and we therefore cannot extract a Luttinger liquid parameter. We can observe CDW order for a range of U_{12}/U in Fig. 6. According to Eq. (16), this order exists when $K_S+K_A<2$. In fact, it coexists with the SF, the PSF, or the CFSF order. At half-filling, K_S will go to zero at a critical positive value of U_{12}. This indicates the transition from the SF-to-CFSF phase.

Finite-size effect. The behavior of $K_{A/S}$ stated above is affected by the size of the system. Finite-size effects can "smooth out" a sudden change in $K_{A/S}$ at the phase transition. This effect can be estimated from the RG flow calculation by integrating Eqs. (8) and (9) out to a finite value l rather than to infinity. In Fig. 6(b), we show an example of a finite-l RG calculation in the vicinity of the PSF-to-SF transition. We see that as l increases, K_A dramatically changes for the attractive U_{12}. In the limit of $l \to \infty$, the RG calculation predicts that K_A becomes discontinuous and "jumps" from 0 to 1 at $U_{12}\approx-0.01U$. This is where the PSF-to-SF transition occurs. This transition is a Berezinskii-Kosterlitz-Thouless transition for which the jump of K_A is well established for an infinite system [11,27]. In order to compare the RG result with our TEBD result, we associate the system size N with the flow parameter l, based on the relation in Eq. (10). The cutoff r_0 is the lattice constant a_L and $r_0'=Na_L$. For $N=80$ we have $l=4.4$ and we find that the RG and the TEBD are in good agreement. The regime between $U_{12}/U\approx-0.06$ and -0.01 is a crossover regime due to the finite size of the system.

Collapse and phase separation. For large $|U_{12}|$, the system approaches collapse or phase separation. According to the Tomonaga-Luttinger liquid theory, $K_S \to \infty$ as the system approaches collapse and $K_A \to \infty$ as the system approaches phase separation. As seen in Fig. 6, we find such a tendency in our TEBD calculations. When U_{12} approaches U, we find that R_A approaches a constant for large distances instead of decaying to zero. We therefore determine the PS regime based on the non-decaying behavior of R_A. In the phase separation regime, $G(x)$ has algebraic decay except for $\nu=0.5$ or 1, where it has exponential decay. An algebraic decay implies two spatially separated single-species superfluids while
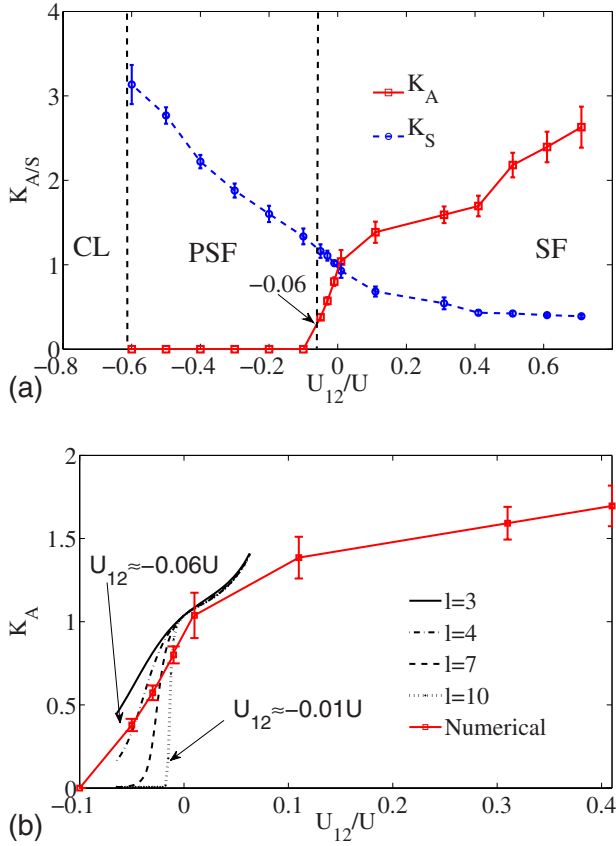
FIG. 6. (Color online) (a) K_S and K_A as functions of U_{12} as extracted from the fit of the correlation functions, R_S and R_A. The filling ν is 0.7 and t/U is 0.02. For $U_{12}/U \lesssim -0.2$ we use a 40-site system. Around $U_{12}/U \approx -0.06$, the antipair correlation function changes from algebraic to exponential decay. This corresponds to the transition from the PSF to the SF phase. When R_A decays exponentially, K_A is formally set to zero. For $K_A + K_S \lesssim 2$, $\alpha_{CDW} = 2 - (K_A + K_S)$ is positive, and the system has CDW order. Error bars are one standard deviation uncertainties obtained from the power-law fit to the numerical data. (b) A comparison of K_A obtained from our RG and TEBD calculations. The red squares connected by lines are the TEBD results while all other lines are determined from the RG flow with flow parameter $l = 3$, 4, 7, and 10, where l is the logarithm of the number of sites [Eq. (10)]. The error bars are as in (a). The PSF-to-SF transition obtained from TEBD is around $U_{12}/U \approx -0.06$, while the RG calculation shows that, for $l = 10$, the transition occurs near $U_{12}/U \approx -0.01$. We interpret the regime between $U_{12}/U \approx -0.06$ and -0.01 the crossover region.

the exponential decay implies two spatially separated Mott insulators [29]. When U_{12} approaches $-U$, R_S does not approach a constant; instead, we observe an inhomogeneous peaked density distribution, indicating collapse.

A. Phase diagram

We study the phase diagram as a function of filling ν and parameters of the Hubbard Hamiltonian. Assuming a positive U, the system can be fully characterized in terms of ν, t/U, and U_{12}/U. Our results are shown in Fig. 7 for a fixed hopping parameter and in Fig. 8 for half-filling.

1. Phase diagram at a fixed hopping parameter

In Fig. 7 we show the phase diagram for filling fractions between 0 and 1 and the interaction U_{12}/U between -1.1 and 1.1. The symbols correspond to numerical data points at which the phases have been characterized. Different markers represent the different orders. The orders are determined from the decay behavior of the three correlation functions R_A, R_S, and G.

For weak attractive interspecies interactions, $-0.06 < U_{12}/U < 0$, the system is in a SF state. As U_{12} grows more attractive, PSF occurs. The critical U_{12} is largest, $\sim -0.08U$, at half-filling and gradually decreases away from half-filling. This phase boundary differs from that predicted by our RG calculation [Eq. (20)], plotted as the dotted line in Fig. 7. This discrepancy is the result of the finite-size effect discussed in Fig. 6(b). In the SF-to-PSF crossover regime, CDW order can coexist. According to the phase diagram in Fig. 3, for attractive interactions, CDW order can coexist only with PSF order. In our numerical work, we observed the CDW order slightly outside the numerical phase boundary of PSF but within the RG phase boundary of PSF. The subregime where CDW and PSF coexist ends when $U_{12}/U \lesssim -0.4$. When the interspecies attraction is comparable to the intraspecies repulsion, $U_{12} \lesssim -U$, the system collapses and no long-range order is present.

For repulsive interspecies interaction and $U_{12} < U$, the system is in a SF state for all noncommensurate fillings. Within the SF regime, there is a smaller parameter region where CDW order coexists with the SF order. This subregime is a quasisupersolid regime. The boundary between a normal superfluid and a quasisupersolid is estimated by RG calculation in Ref. [20]. At half-filling, CFSF occurs when $0.08 \lesssim U_{12}/U \lesssim 1$. Within the CFSF regime, the CDW order can coexist, forming a quasisupersolid of antipairs. It also worthwhile to point out that, at half-filling, CDW order only exists within the PSF and the CFSF regimes. At unit filling, our numerical results do not show evidence of PSF or CFSF for any U_{12}. We find a MI state for $|U_{12}| < U$.

2. Phase diagram at half-filling

In Fig. 8, we show the phase diagram at half-filling as a function of U_{12}/U and t/U. From this diagram, we find that the border between PSF and SF and the border between PSF and CL approach each other as t increases. Similarly, the border between the CFSF and SF and the border between CFSF and PS approach each other. In fact, the PSF and the CFSF phases end around $t \sim 0.16U$. Within the PSF and the CFSF regimes, CDW order can coexist. In the phase separated regime, the separated single-species ensembles form two individual Mott insulating states for $t \lesssim 0.14U$ and two individual SF states for $t > 0.14U$.

We can compare this phase diagram with the half-filling phase diagram in Fig. 4 obtained from the Tomonaga-Luttinger liquid theory. Especially, we can compare the location of the phase boundary between SF and PSF (CFSF). To do so, we plot the RG phase boundaries, described by Eqs. (20) and (24), onto our phase diagram. The area near the two boundaries is interpreted as the crossover regime where finite-size effects modify the phase boundary.
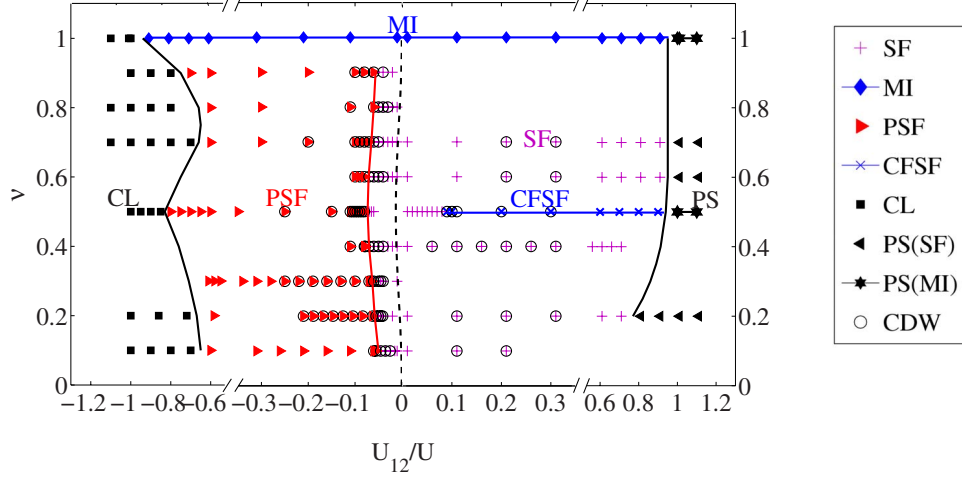
FIG. 7. (Color online) Phase diagram for a homogeneous system and the hopping parameter $t=0.02U$ as a function of filling ν and interspecies interaction U_{12}/U. The horizontal axis shows three disconnected regions in U_{12}/U. The solid lines are the estimated phase boundaries based on the TEBD results and the dotted line is the PSF-to-SF phase boundary predicted by our RG calculation [see Eq. (20)]. For attractive interaction $U_{12} \lesssim -0.06U$, the system forms a PSF. The state collapses (CL) for $U_{12} \lesssim -0.7U$. For $U_{12} \gtrsim -0.06$ and $U_{12} \lesssim U$ the system shows single-particle superfluidity (SF). The system phase separates (PS) for $U_{12} \gtrsim 1$ and forms two single-particle superfluids (SF). Open circles are the points where $K_S + K_A < 2$ and CDW order coexists with a superfluid phase (SF, PSF, or CFSF). At half-filling and unit filling there exist special phases. For repulsive interaction $U_{12} \gtrsim 0.08U$ and half-filling, the system forms a CFSF. For unit filling, we find a Mott-Insulator (MI) phase for interactions $|U_{12}| \lesssim U$. Finally, in the PS region at half-filling and unit filling, the system forms two individual MI states. For $\nu = 0.9, 0.8, 1$ and $\nu = 0.7$, $U_{12}/U \leq -0.2$, the calculation is performed for a 40-site system.

B. Realization and detection

Having established the phase diagram for the homogeneous system, we now discuss how to realize and detect the PSF and the CFSF phases. First, we need to modify the Hubbard Hamiltonian in Eq. (1) because in any ultracold atom experiment an additional trapping potential is present. We add a harmonic potential $\Omega(j - j_c)^2(n_{1,j} + n_{2,j})$, where j is the site index and j_c is the index at the center of the system. The TEBD method is used to find the ground state. We consider a system of 80 lattice sites and adjust the total number of particles and the trap frequency, so that the number of particles is negligible at the edge of the lattice.

We again determine the orders of the system by studying the correlation functions in Table I. We find that, in spite the presence of the trap, the correlation functions still show exponential or algebraic scaling away from the edge of the lattice. In fact, a correlation function can have different decay behavior in different parts of the trap. We also find that SF, PSF, and CFSF still exist. The remainder of this paper focuses on experimental signatures that distinguish between these orders by calculating the density distribution, the time-
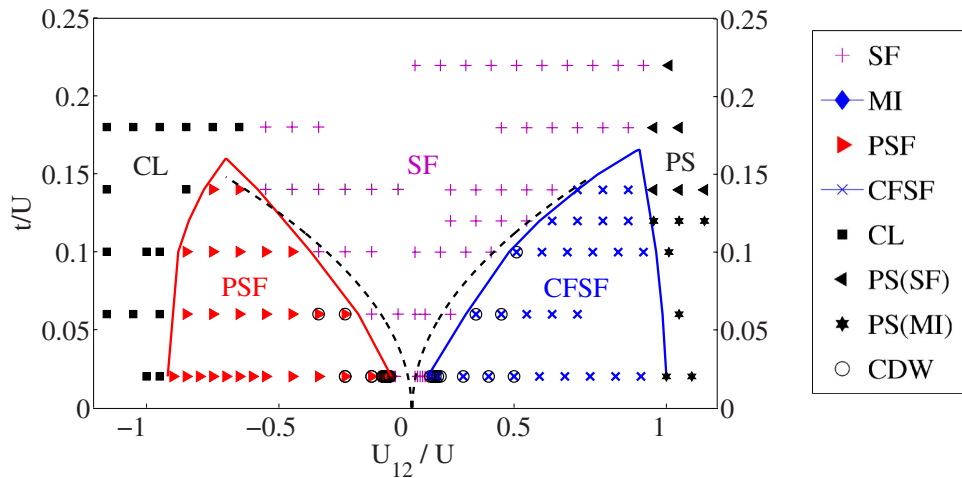
FIG. 8. (Color online) Phase diagram at half-filling as a function of U_{12}/U and t/U. The solid lines are estimated phase boundaries from the TEBD calculation and the dotted lines are the phase boundaries predicted by the RG calculation [see Eqs. (20) and (24)]. For large repulsive interaction, the system phase separates (PS) and for large attractive interaction, the system collapses (CL). For moderate interactions and for $t/U \lesssim 0.2$, the system shows PSF on the attractive side and counterflow superfluidity on the repulsive side. Both PSF and CFSF can coexist with CDW order when $t \lesssim 0.1U$. For $t = 0.14, -0.18$ and $t = 0.1$, $U_{12}/U \leq -0.15$, the calculation is performed in a 40-site system.

(a)   (b)
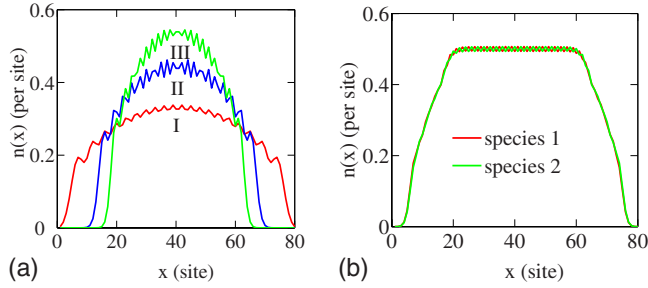
FIG. 9. (Color online) Density distribution of a trapped system for $t=0.02U$. (a) Attractive interaction U_{12}. The trap frequency is $\Omega=1\times10^{-5}U$ and the number of atoms is 20 for each species. For attractive interactions, the density distributions of the two species are identical. For $U_{12}=-0.01U$ (curve I) the system is superfluid. For $U_{12}=-0.11U$ (curve II) and $U_{12}=-0.21U$ (curve III), the system is in the PSF state. As U_{12} becomes more negative, the distribution gradually shrinks in size. (b) Repulsive interaction $U_{12}=0.2U$ with $\Omega=8\times10^{-5}U$ and 30 atoms of each species. The red and the green curves correspond to the species, respectively. The density distribution has a plateau with half-filling in the center of the trap. The system is in a CFSF state. The two species have weak interlocked density modulations around half-filling.

of-flight image after an expansion, or the structure factor for Bragg spectroscopy.

1. Density distribution

Due to the presence of trap, the density distribution is not homogeneous. We find that PSF can exist at the places where the local density of each species is less than one atom per site or equivalently per lattice constant a_L. On the other hand, CFSF can only exist when the local density is exactly 1/2 atom per site.

In Fig. 9(a) we show density distributions for three attractive interactions U_{12} and a hopping parameter equal to the one used for Fig. 7. For all attractive interactions, the density distributions of each species are the same. For more attractive interspecies interaction, the density distribution concentrates near the center of the trap. There is no discontinuous change in the density distribution when the system goes from SF to PSF.

In Fig. 9(b) we show the density distribution for $U_{12}=0.2U$. In this case, in the center of the trap, where the density distribution is constant or has a "plateau," the system is in a CFSF state. The plateau is at half-filling consistent with predictions from a local-density approximation and noting that in Fig. 7 CFSF only occurs at $\nu=1/2$. Toward the edge, where the density is decreasing sharply, it is in a SF state. The plateau implies that the system is incompressible in the center. Indeed, as we discussed in Sec. III, the CFSF phase has a vanishing compressibility of the total density, related to the presence of a "charge gap" in the CFSF state [11].

2. Time-of-flight measurement

A widely used measurement technique in the field of ultracold atoms is measuring the density of atoms after a TOF

(a)   (b)
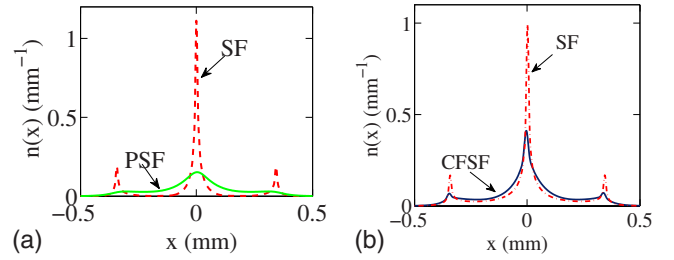
FIG. 10. (Color online) Density distribution after a time-of-flight expansion. We assume ^{87}Rb atoms and use an expansion time of 0.03 s. The hopping energy is $t=0.02U$. (a) For attractive interaction U_{12}, we show the TOF expansion of a SF state at $U_{12}=-0.01U$ (red line) and of a PSF state at $U_{12}=-0.21U$ (green line). The two curves correspond to the expansion of the densities shown as curves I and III in Fig. 9(a). The trap frequency is $\Omega=1\times10^{-5}U$. (b) For repulsive interaction, we show a TOF expansion of a SF state at $U_{12}=0.01U$ and of a CFSF state at $U_{12}=0.21U$. The trap frequency is $\Omega=8\times10^{-5}U$.

expansion. The 1D optical lattice potential and the harmonic trap are abruptly turned off at time $T=0$ and the atoms expand freely afterward. We calculate the density at time T, according to

$$n_a(x,T) = \langle c_a^\dagger(x,T)c_a(x,T)\rangle \qquad (32)$$

with $a=1,2$. The operators $c_a(x,T)$ are related to the lattice operator $b_{a,j}$ according to

$$b_a(x,T) = \sum_{j=1}^{N} w(x-r_j,T)b_{a,j}, \qquad (33)$$

where $w(x,T)=\sqrt{d/\sqrt{2\pi\Delta(T)^2}}\exp\{-x^2/[4\Delta(T)^2]\}$ describes the free expansion from the initial Gaussian wave function of an atom in a lattice site and $\Delta(T)^2=d^2+iT\hbar/(2m)$. The parameter d is the width of the initial Gaussian state and m is the atomic mass. The density distribution $n_a(x,T)$ is then given by

$$n_a(x,T) = \sum_{j_1,j_2=1}^{N} w^*(x-r_{j_1},T)w(x-r_{j_2},T)G(j_1,j_2),$$

where $G(j_1,j_2)$ is the single-particle Green's function. In Fig. 10 we show examples of TOF expansions of PSF, CFSF, and SF orders. For the SF phase, we find a strongly peaked interference pattern, reflecting the single-particle quasi-long-range order. For both PSF and CFSF phases, the TOF density shows a broad Lorentzian distribution, which is due to the exponential decay of the single-particle Green's function.

3. Feshbach ramp

In order to detect the superfluidity of pairs, we consider applying a Feshbach ramp to pairwise project the atoms onto molecules formed by one atom from each species, which is similar to detection of fermionic pairs in the BCS regime [4]. In those experiments, a fast ramp across a Feshbach resonance was used, followed by a time-of-flight expansion. The
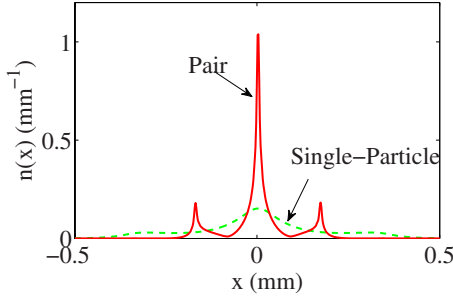
FIG. 11. (Color online) Density distribution of molecules after time-of-flight expansion of state III in Fig. 9(a). The expansion time is 0.03 s. We assume two hyperfine states of ^{87}Rb. These are converted into Feshbach molecules at $T=0$ via a fast ramp across a resonance. We assume a complete conversion. The strongly peaked interference pattern of molecules indicates the presence of a quasi-condensate of pairs. For comparison, we also show the TOF expansion of atoms in the PSF phase for the same parameters. The broad Lorentzian distribution demonstrates the absence of single-particle SF.

density distribution of the molecules showed the superfluidity of fermionic pairs. We propose a similar detection for bosonic pairs in PSF.

To give a simple estimate of a TOF image after a Feshbach ramp, we imagine that bosons of different species on the same lattice site are converted into molecules. This leads to the replacement $b_{1,j}b_{2,j} \rightarrow M_j$, where M_j is the molecule annihilation operator. A TOF density of the molecules at position x and time T is given by

$$n_M(x,T) = \sum_{j_1,j_2=1}^{N} w^*(x-r_{j_1},T)w(x-r_{j_2},T)R_s(j_1,j_2).$$

(34)

In the expanding wave function $w(x,T)$, the mass m is replaced with the mass of the molecule. We assume the same initial width d. In a more realistic estimate, the conversion efficiency to molecules would not be 100%, but approximately given by the square of the overlap of the molecular wave function and the single-atom wave functions. This leads to a reduced signal. The spatial dependence, however, remains the same. In Fig. 11, we see an example of the density of molecules after TOF and, for comparison, the atomic density after TOF for the PSF state. The strongly peaked molecular distribution indicates the quasicondensate of the bosonic pairs. The single-atom density is a broad Lorentzian distribution, indicating the absence of single-particle SF.

4. Bragg spectroscopy

To detect the presence of CDW order, one can use Brag spectroscopy [30,31]. The quantity that is measured in those experiments is either the dynamic or the static structure factor. Here, we calculate the static structure factor $S_a(k)$ for species $a=1,2$. It is defined as
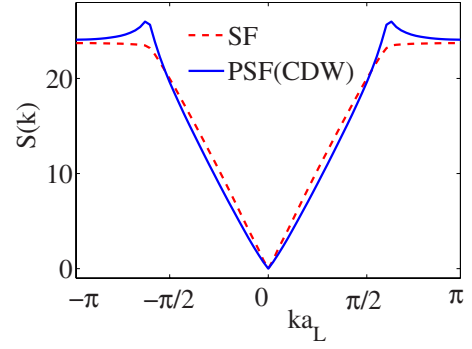
FIG. 12. (Color online) Structure factor at filling $\nu=0.3$. For $U_{12}=-0.01U$ the system is in the SF regime (dashed line) and for $U_{12}=-0.07U$ the system is in the PSF regime (continuous line). Cusps at $|k|=2\pi\nu$ only occur for $U_{12}=-0.07U$ indicating the coexistence of CDW with PSF order.

$$S_a(k) = \frac{1}{N}\sum_{j_1,j_2} e^{-ika_L(j_1-j_2)}[\langle n_a(j_1)n_a(j_2)\rangle - \langle n_a(j_1)\rangle\langle n_a(j_2)\rangle].$$

(35)

For wave vectors k near twice the "Fermi wave vector" k_F, the structure factor $S(k) \sim ||k|-2k_F|^{1-\alpha_{CDW}}$ with $\alpha_{CDW}=2-K_S-K_A$ [11]. In our system, K_S+K_A is always larger than 1 and, thus, $1-\alpha_{CDW}$ is positive. Consequently, the structure factor does not diverge. In the CDW regime with $K_S+K_A<2$ the power $1-\alpha_{CDW}$, however, is less than 1. This gives $S(k)$ cusps at $\pm 2k_F$ when CDW quasi-long-range order is present. In Fig. 12 we show examples of $S(k)$ for a case with and without CDW.

5. Bragg spectroscopy preceded by a $\pi/2$ pulse

To detect CFSF order, we propose the following detection method. It applies to the case that the mixture is composed of atoms in different internal states rather than different atomic species [33]. First, we apply a $\pi/2$ pulse, which transfers the atoms into the superpositions $b_{1/2,i} \rightarrow b_{\pm,i}=(b_{1,i} \pm b_{2,i})/\sqrt{2}$. We then measure the structure factor, which now corresponds to the Fourier transform of the density correlations $R_{n\pm}(i,j)=\langle n_{\pm,i}n_{\pm,j}\rangle - \langle n_{\pm,i}\rangle\langle n_{\pm,j}\rangle$. In terms of the original
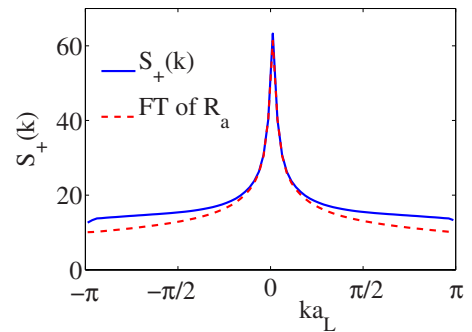
FIG. 13. (Color online) Structure factor $S_+(k)$ (blue line) after applying a $\pi/2$ pulse in the CFSF phase. The quasicondensate of antipairs generates an algebraic peak at $k=0$. The peak also appears in the Fourier transform of the antipair correlation function $R_a(i,j)=\langle b^\dagger_{1,i}b_{2,i}b^\dagger_{2,j}b_{1,j}\rangle$ (red dashed line).

$b_{1/2,i}$, operators these density correlations are given by

$$R_{n\pm}(i,j) = \frac{1}{4}\langle (n_{1,i} + n_{2,i})(n_{1,j} + n_{2,j})\rangle - \frac{1}{4}(\langle n_{1,i}\rangle + \langle n_{2,i}\rangle)(\langle n_{1,j}\rangle$$

$$+ \langle n_{2,j}\rangle) + \frac{1}{2}\langle b_{1,i}^\dagger b_{2,i} b_{2,j}^\dagger b_{1,j}\rangle. \tag{36}$$

The last term in the above equation is the correlation function $R_a(i,j)$ of the order parameter of CFSF, $b_{1,j} b_{2,j}^\dagger$. In Fig. 13, we show the structure factor $S_+(k)$, the Fourier transform of Eq. (36), as well as the Fourier transform of $R_a(i,j)$. Both $S_+(k)$ and the Fourier transform of $R_a(i,j)$ have a cusp around $k=0$. The cusp is due to the long-range correlations of the antipairs in the CFSF. The two functions are nearly identical near $k=0$, indicating that the momentum distribution of antipairs can be measured by determining the structure factor $S_+(k)$.

V. SUMMARY

We have studied ground-state properties of one-dimensional Bose mixtures in an optical lattice using both the Tomonaga-Luttinger liquid theory and the time-evolving block decimation method. We first discussed the zero-temperature phase diagram in a homogeneous system at different filling fractions and different parameter regimes. We have shown that 1D Bose mixtures in an optical lattice can have quasi-long-range orders that include superfluid, paired superfluid (PSF), counterflow superfluid (CFSF), and Mott insulator. We also found that each type of superfluid order can coexist with charge-density wave (CDW) order and that in both PSF and CFSF phases single-particle superfluidity (SF) is absent.

In addition, we discussed ways of realizing and detecting these phases experimentally. We propose using a Feshbach ramp to probe the momentum distribution of pairs in the PSF, which shows signatures of the quasicondensate of pairs. To detect the CFSF for a mixture composed of two atomic hyperfine states, we propose to measure the static structure factor by using Bragg spectroscopy preceded by a $\pi/2$ pulse. A sharp peak in the structure factor was shown to be dominated by the contribution from the momentum distribution of antipairs in the CFSF phase. Finally, we suggest to detect CDW order with Bragg spectroscopy.

ACKNOWLEDGMENTS

APPENDIX: TEBD METHOD FOR TWO-SPECIES MANY-BODY SYSTEMS

In this appendix, we briefly review the time-evolving block decimation (TEBD) method [14] used in Sec. IV and explain an efficient way to apply the TEBD to a two-species Bose-Hubbard model. We use the number-conserving version of the TEBD method [15].

The TEBD determines the ground state via an imaginary time evolution for one-dimensional (1D) quantum lattice systems. In this method the Hilbert space **H** is decomposed as

$$\mathbf{H} = \otimes_{l=1}^{M}\mathbf{H}_l. \tag{A1}$$

Here, l refers to the lth lattice site, M is the number of sites, and $\mathbf{H}_l$ is the local Hilbert space at site l with local dimension d, independent of l. Any state $|\Psi\rangle$ in **H** is represented as

$$|\Psi\rangle = \sum_{j_1,j_2,\ldots,j_M=1}^{d} c_{j_1,j_2,\ldots,j_M}|j_1\rangle|j_2\rangle\cdots|j_M\rangle. \tag{A2}$$

In the TEBD algorithm, coefficients $c_{j_1,j_2,\ldots,j_M}$ are decomposed as

$$c_{j_1,j_2,\ldots,j_M} = \sum_{\alpha_1=1}^{\chi_1}\sum_{\alpha_2=1}^{\chi_2}\cdots\sum_{\alpha_{M-1}=1}^{\chi_{M-1}}\Gamma_{\alpha_1}^{[1]j_1}$$

$$\times\lambda_{\alpha_1}^{[1]}\Gamma_{\alpha_1\alpha_2}^{[2]j_2}\lambda_{\alpha_2}^{[2]}\cdots\lambda_{\alpha_{M-2}}^{[M-2]}\Gamma_{\alpha_{M-2}\alpha_{M-1}}^{[M-1]j_{M-1}}\lambda_{\alpha_{M-1}}^{[M-1]}\Gamma_{\alpha_{M-1}}^{[M]j_M}. \tag{A3}$$

The variables $\lambda_{\alpha_l}^{[l]}$ and χ_l are the Schmidt coefficients and rank of the Schmidt decomposition of $|\Psi\rangle$ with respect to the bipartite splitting of the system into $[1,\ldots,l-1,l]:[l+1,l+2,\ldots,M]$,

$$|\Psi\rangle = \sum_{\alpha_l=1}^{\chi_l}\lambda_{\alpha_l}^{[l]}|\Phi_{\alpha_l}^{[1,\ldots,l-1,l]}\rangle|\Phi_{\alpha_l}^{[l+1,l+2,\ldots,M]}\rangle. \tag{A4}$$

We take $\lambda_\alpha^{[l]} > \lambda_\beta^{[l]}$ for all $\alpha < \beta$. In one dimension, the rank χ_l at the center of the system must be on the order of $d^{M/2}$ in order to express arbitrary states. However, since it is empirically known that the Schmidt coefficients $\lambda_\alpha^{[l]}$ decrease rapidly with index α for the ground and the low-lying excited states, we set χ_l to a relatively small number χ for all l.

To efficiently simulate the two-species Bose-Hubbard model [Eq. (1) in the main text], we map it onto the one-species Hamiltonian

$$H = -t\sum_{l=1}^{2N-2}(b_l^\dagger b_{l+2} + \text{H.c.}) + U_{12}\sum_{\text{odd }l} n_l n_{l+1} + \frac{U}{2}\sum_{l=1}^{2N} n_l(n_l - 1), \tag{A5}$$

where N is the number of sites in the original two-species Hamiltonian. In this one-species Hamiltonian, there are $2N$ sites, each of which is indexed by l. The odd sites l correspond to species 1 and the even sites to species 2. Hopping between neighboring sites $-tb_{a,i}^\dagger b_{a,i+1}$ in Eq. (1) is mapped onto a next-nearest-neighbor hopping $-tb_l^\dagger b_{l+2}$ in Eq. (A5). Similarly, the interspecies on-site interaction $U_{12} n_{1,i} n_{2,i}$ is mapped onto the nearest-neighbor interaction $U_{12} n_l n_{l+1}$. This type of mapping has been successfully applied to treat the two-legged Bose-Hubbard model [16].

We map the two-species Bose-Hubbard Hamiltonian (1) onto the one-species Hamiltonian because it reduces the computational cost dramatically. This cost in TEBD [14] scales as $Md^3\chi^3$. For the two-species system with N sites we must define a dimension of the local Hilbert space for each species, say D. Hence, at each site there are D^2 basis functions and the cost scales as ND^6. On the other hand, for the mapped Hamiltonian with $2N$ sites and a local dimension D

the cost only scales as $2ND^3$. In our calculation, we set $d=3$ for the filling factor $\nu \leq 0.8$ and $d=5$ for $\nu=0.9, 1$. In this case, the mapping makes the computation five to ten times faster.

The imaginary time evolution of any state to the ground state is given by the repeated application of $e^{-iH\delta}$ on $|\Psi\rangle$, where δ is a small imaginary time step. To apply this operator, we first split the Hamiltonian into three parts as $H = H_{\text{int}} + H_{\text{hop}}^{\text{odd}} + H_{\text{hop}}^{\text{even}}$, where

$$H_{\text{int}} = \sum_{m=1}^{N} \left[U_{12} n_{2m-1} n_{2m} + U n_{2m-1}(n_{2m-1} - 1) \right.$$
$$\left. + U n_{2m}(n_{2m} - 1) \right],$$

$$H_{\text{hop}}^{\text{odd}} = -t \sum_{\text{odd } m} (b_{2m-1}^{\dagger} b_{2m+1} + b_{2m}^{\dagger} b_{2m+2} + \text{H.c.}),$$

$$H_{\text{hop}}^{\text{even}} = -t \sum_{\text{even } m} (b_{2m-1}^{\dagger} b_{2m+1} + b_{2m}^{\dagger} b_{2m+2} + \text{H.c.}). \quad \text{(A6)}$$

Subsequently, we use the second-order Suzuki-Trotter expansion to decompose $e^{-i\hat{H}\delta}$ as

$$e^{-iH\delta} = e^{-iH_{\text{int}}\delta/2} e^{-iH_{\text{hop}}^{\text{odd}}\delta/2} e^{-iH_{\text{hop}}^{\text{even}}\delta} e^{-iH_{\text{hop}}^{\text{odd}}\delta/2} e^{-iH_{\text{int}}\delta/2} + O(\delta^3). \quad \text{(A7)}$$

Each of the operators $e^{-iH_{\text{int}}\delta/2}$, $e^{-iH_{\text{hop}}^{\text{odd}}\delta/2}$, and $e^{-i\hat{H}_{\text{hop}}^{\text{even}}\delta}$ can be decomposed into a product of two-site operators, which can be efficiently applied to the matrix product state $|\Psi\rangle$ [14,17,32]. We use swapping techniques to apply the next-nearest-neighbor operators $e^{-iH_{\text{hop}}^{\text{odd}}\delta/2}$ and $e^{-i\hat{H}_{\text{hop}}^{\text{even}}\delta}$ [17,32,33].

[1] S. Bose, Z. Phys. **26**, 178 (1924); A. Einstein, Sitzungsber. Preuss. Akad. Wiss., Phys. Math. Kl. **1924**, 261; **1925**, 3.

[2] K. B. Davis, M.-O. Mewes, M. R. Andrews, N. J. van Druten, D. S. Durfee, D. M. Kurn, and W. Ketterle, Phys. Rev. Lett. **75**, 3969 (1995); M. H. Anderson, J. R. Ensher, M. R. Matthews, C. E. Wieman, and E. A. Cornell, Science **269**, 198 (1995); C. C. Bradley, C. A. Sackett, J. J. Tollett, and R. G. Hulet, Phys. Rev. Lett. **75**, 1687 (1995).

[3] L. N. Cooper, Phys. Rev. **104**, 1189 (1956); J. Bardeen, L. N. Cooper, and J. R. Shrieffer, *ibid.* **106**, 162 (1957); **108**, 1175 (1957).

[4] C. A. Regal, M. Greiner, and D. S. Jin, Phys. Rev. Lett. **92**, 040403 (2004); M. W. Zwierlein, C. A. Stan, C. H. Schunck, S. M. F. Raupach, A. J. Kerman, and W. Ketterle, *ibid.* **92**, 120403 (2004); M. Bartenstein, A. Altmeyer, S. Riedl, S. Jochim, C. Chin, J. H. Denschlag, and R. Grimm, *ibid.* **92**, 120401 (2004); T. Bourdel, L. Khaykovich, J. Cubizolles, J. Zhang, F. Chevy, M. Teichmann, L. Tarruell, S. J. J. M. F. Kokkelmans, and C. Salomon, *ibid.* **93**, 050401 (2004).

[5] A. B. Kuklov and B. V. Svistunov, Phys. Rev. Lett. **90**, 100401 (2003).

[6] A. Kuklov, N. Prokof'ev, and B. Svistunov, Phys. Rev. Lett. **92**, 050402 (2004); **92**, 030403 (2004).

[7] D. Jaksch, C. Bruder, J. I. Cirac, C. W. Gardiner, and P. Zoller, Phys. Rev. Lett. **81**, 3108 (1998).

[8] M. Greiner, O. Mandel, T. Esslinger, T. W. Hänsch, and I. Bloch, Nature (London) **415**, 39 (2002).

[9] T. Stöferle, H. Moritz, C. Schori, M. Köhl, and T. Esslinger, Phys. Rev. Lett. **92**, 130403 (2004).

[10] I. B. Spielman, W. D. Phillips, and J. V. Porto, Phys. Rev. Lett. **98**, 080404 (2007).

[11] T. Giamarchi, *Quantum Physics in One Dimension* (Oxford University Press, Oxford, UK, 2004).

[12] B. Paredes, A. Widera, V. Murg, O. Mandel, S. Foelling, I. Cirac, G. Shlyapnikov, T. W. Hansch, and I. Bloch, Nature (London) **429**, 277 (2004).

[13] A. Widera, S. Trotzky, P. Cheinet, S. Fölling, F. Gerbier, I. Bloch, V. Gritsev, M. D. Lukin, and E. Demler, Phys. Rev. Lett. **100**, 140401 (2008).

[14] G. Vidal, Phys. Rev. Lett. **98**, 070201 (2007); **91**, 147902 (2003); **93**, 040502 (2004); S. R. White and A. E. Feiguin, *ibid.* **93**, 076401 (2004).

[15] A. J. Daley, S. R. Clark, D. Jaksch, and P. Zoller, Phys. Rev. A **72**, 043618 (2005); A. J. Daley, Ph.D. thesis, Leopold-Franzens-Universität Innsbruck, 2005.

[16] I. Danshita, J. E. Williams, C. A. R. Sá de Melo, and C. W. Clark, Phys. Rev. A **76**, 043606 (2007); I. Danshita, C. A. R. Sá de Melo, and C. W. Clark, *ibid.* **77**, 063609 (2008).

[17] I. Danshita and P. Naidon, Phys. Rev. A **79**, 043601 (2009).

[18] A. Argüelles and L. Santos, Phys. Rev. A **75**, 053613 (2007); **77**, 059904(E) (2008).

[19] L. Mathey, Phys. Rev. B **75**, 144510 (2007).

[20] L. Mathey, I. Danshita, and C. W. Clark, Phys. Rev. A **79**, 011602(R) (2009).

[21] G. G. Batrouni, F. Hébert, and R. T. Scalettar, Phys. Rev. Lett. **97**, 087209 (2006); V. W. Scarola and S. Das Sarma, *ibid.* **95**, 033003 (2005); P. Sengupta, L. P. Pryadko, F. Alet, M. Troyer, and G. Schmid, *ibid.* **94**, 207202 (2005); S. Wessel and M. Troyer, *ibid.* **95**, 127205 (2005); D. Heidarian and K. Damle, *ibid.* **95**, 127206 (2005); R. G. Melko, A. Paramekanti, A. A. Burkov, A. Vishwanath, D. N. Sheng, and L. Balents, *ibid.* **95**, 127207 (2005); H. P. Büchler and G. Blatter, *ibid.* **91**, 130404 (2003); M. Boninsegni and N. Prokof'ev, *ibid.* **95**, 237204 (2005); M. Boninsegni, J. Low Temp. Phys. **132**, 39 (2003); D. L. Kovrizhin, G. Venketeswara Pai, and S. Sinha, EPL **72**, 162 (2005); F. Karim Pour, M. Rigol, S. Wessel, and A. Muramatsu, Phys. Rev. B **75**, 161104(R) (2007).

[22] C. Trefzger, C. Menotti, and M. Lewenstein, Phys. Rev. Lett. **103**, 035304 (2009).

[23] A. Masaki, S. Tsukada, and H. Mori, J. Phys.: Conf. Ser. **150**, 032050 (2009).

[24] F. D. M. Haldane, Phys. Rev. Lett. **47**, 1840 (1981).

[25] M. A. Cazalilla, J. Phys. B **37**, S1 (2004).

[26] M. A. Cazalilla, Phys. Rev. A **70**, 041604(R) (2004).

[27] J. M. Kosterlitz and D. J. Thouless, J. Phys. C **6**, 1181 (1973); V. L. Berezinskii, Zh. Eksp. Teor. Fiz. **6**, 907 (1970) [Sov.

Phys. JETP **32**, 493 (1971)].

[28] J. B. Kogut, Rev. Mod. Phys. **51**, 659 (1979).

[29] T. Mishra, R. V. Pai, and B. P. Das, Phys. Rev. A **76**, 013604 (2007).

[30] J. Stenger, S. Inouye, A. P. Chikkatur, D. M. Stamper-Kurn, D. E. Pritchard, and W. Ketterle, Phys. Rev. Lett. **82**, 4569 (1999); J. Steinhauer, R. Ozeri, N. Katz, and N. Davidson, *ibid.* **88**, 120407 (2002).

[31] D. Clément, N. Fabbri, L. Fallani, C. Fort, and M. Inguscio, Phys. Rev. Lett. **102**, 155301 (2009).

[32] Y.-Y. Shi, L.-M. Duan, and G. Vidal, Phys. Rev. A **74**, 022320 (2006).

[33] D. S. Hall, M. R. Matthews, C. E. Wieman, and E. A. Cornell, Phys. Rev. Lett. **81**, 1543 (1998).